GEOPHYSICS, VOL. 76, NO. 4 (JULY-AUGUST 2011); P. T65–T78, 18 FIGS.
10.1190/1.3581360

Improving the efficiency of elastic wave-mode separation for heterogeneous tilted transverse isotropic media

Jia Yan[1] and Paul Sava[2]

ABSTRACT

Wave-mode separation for TI (transversely isotropic) models can be carried out by nonstationary filtering the elastic wavefields with localized filters. These filters are constructed based on the polarization vectors obtained by solving the Christoffel equation using local medium parameters. This procedure, although accurate, is computationally expensive, especially in 3D. We develop an efficient method for wave-mode separation, which exploits the same general idea of projecting wavefields onto polarization vectors. The method consists of two steps: (1) separate wave modes in the wavenumber domain at a number of reference models to obtain the same number of partially separated wavefields; then transform all the wavefields to the space domain; (2) interpolate the wavefields (obtained in step 1) in the space domain using the spatially-variable model parameters. The new method resembles the phase-shift plus interpolation (PSPI) technique, which interpolates the wavefields that are reconstructed at several reference velocities. Synthetic examples indicate that the separation followed by interpolation is effective for models with complex geology. The new technique has the benefits of speed and accuracy.

INTRODUCTION

In geophysical exploration, seismic waves propagate in the earth as a superposition of compressional and shear modes. Conventional acoustic migration techniques that ignore the shear modes usually suffice for structural imaging. However, in areas where the P-wave is strongly attenuated, e.g,. in a gas plume (Stewart et al., 2003), converted-wave migration may aid in imaging of these regions. Multicomponent data are acquired on land and at ocean bottom for elastic imaging. It is desirable to obtain converted-wave images that resemble conventional acoustic-wave images in physical meaning, i.e., PP and PS images should represent the PP and PS reflection coefficients, respectively. To produce the desired multicomponent images, Yan and Sava (2008) propose to use an imaging condition that crosscorrelates (or deconvolves) source and receiver potentials, which requires wave-mode separation for the reconstructed elastic wavefields. Recently, extensive research has been done on two-way acoustic wave equation that propagates pure P-waves in TTI media (Alkhalifah, 1998; Etgen and Brandsberg-Dahl, 2009; Liu et al., 2009; Fowler et al., 2010). Modeling and imaging with TI acoustic wave equation guarantees simplicity of pure-mode propagation and an acoustic imaging condition. However, imaging with acoustic wave equation does not allow for internal converted waves.

Wave-mode separation for isotropic media can be achieved by applying Helmholtz decomposition to the vector wavefields (Aki and Richards, 2002), which is effective for homogeneous and heterogeneous isotropic media. Dellinger and Etgen (1990) extend wave-mode separation to homogeneous vertically transversely isotropic (VTI) media, and obtain P- and SV-modes by projecting the vector wavefields onto the polarization vectors of different modes in the wavenumber domain. Yan and Sava (2009a,b) extend this technology to heterogeneous VTI and TTI media, respectively; they show that separation is effective even for complex geology with high heterogeneity, if the projection is carried out in the space domain by filtering the vector wavefields with spatially variable operators (Yan and Sava, 2009a,b).

Yan and Sava (2009a,b) show wave-mode separation in symmetry-axis planes of TI media. For heterogeneous models, wave-mode separation can be performed in the space domain using nonstationary spatial filtering, which is computationally expensive. In fact, the cost becomes prohibitive in 3D because it is proportional to the number of grids in the model and the size of each filter (Yan and Sava, 2009a). Zhang and McMechan (2010)

Manuscript received by the Editor 7 September 2010; revised manuscript received 19 January 2011; published online 3 June 2011.
[1]ExxonMobil Upstream Research Company, Houston, Texas, U.S.A. E-mail: jia.yan@exxonmobil.com; hellobettypku@gmail.com.
[2]Colorado School of Mines, Center for Wave Phenomena, Golden, Colorado, U.S.A. E-mail: psava@mines.edu; paul.sava@gmail.com.

separate wave modes for heterogeneous models that are comprised of several distinct geologic units, where the polarization vectors in each unit are stationary. They separate wave modes using medium parameters taken from each unit and obtain a final separation by combining correctly separated modes from corresponding blocks. This approach is only effective when the model has distinct units and when it is easy to choose the separated modes from the corresponding units. When the medium is not comprised of distinct units but has continuously changing model parameters, it is difficult to disassemble the medium to apply the method of Zhang and McMechan (2010).

In this paper, we propose a new approach for wave-mode separation in two steps. First, choose some reference models based on the model parameter distribution and separate wave modes in the wavenumber domain at these reference models. Then, we transform all the separated modes to the space domain. Finally, we interpolate the wavefields in the space domain using the spatially variable model parameters. Our approach is effective for geologic models with a high heterogeneity.

In the following, we show that wave-mode separation can be carried out more efficiently in a mixed domain — separation in the wavenumber domain followed by interpolation in the space domain. This procedure, which resembles the phase-shift plus interpolation (PSPI) process from wave-equation migration (Gazdag and Sguazzero, 1984; Bale et al., 2007; Ursenbach and Bale, 2009), offers speed and accuracy. We use synthetic examples to show that the proposed approach is efficient: we achieve approximately the same accuracy as the space-domain separation and significantly reduce the computational cost.

WAVE-MODE SEPARATION IN THE WAVENUMBER DOMAIN BY INTERPOLATION

As illustrated in Yan and Sava (2009a,b), accurate separation of wave modes for heterogeneous TI media requires nonstationary filtering with large operators in the space domain, which is computationally expensive. The computation cost is directly proportional to the size of the model and the size of the space-domain filters, which are usually large (for example, 50×50 in 2D, in Yan and Sava, 2009b).

For a 3D model of size N_x^3, the cost of filtering with a filter of size n^3 is about

$$\sim 2n^3N_x^3. \tag{1}$$

Here, the filtering cost at each grid point in the model is about n^3 multiplications plus n^3 summations.

If we use wavenumber domain separation followed by interpolation, the cost is due to forward and inverse Fourier transforms, in addition to the multiplications and summations in the k-domain at each reference model:

$$2\left(N_x^3\, log_2\left(N_x^3\right)\right) \times 3 + 2\left(N_x^3\right)N \approx (18\, log_2 N_x + 2N)N_x^3, \tag{2}$$

where N is the number of reference models. One can see that even if a filter has only 20^3 samples, i.e., $n = 20$, and a model is 1000^3, i.e., $N_x = 1000$, by going from Equation 1 to Equation 2 and using 10 reference modes, i.e., $N = 10$, the computation cost is lowered by a factor of about 80.

Furthermore, in a simple implementation, the storage of the separation filters for the entire model is also proportional to the size of the model times the size of the filters $\left(n^3N_x^3\right)$. Thus, the spatial separation becomes prohibitively expensive in 3D.

To mitigate the cost and storage problem, we implement the wave-mode separation in the mixed domain at a much lower cost: the wave modes are first separated at a number of reference models in the wavenumber domain; then the separated modes obtained at these references are interpolated in the space domain. Here, for 3D TTI media, the model space is multi-dimensional:

$$\mathbf{m} = \{V_{P0}, V_{S0}, \varepsilon, \delta, \gamma, \nu, \alpha\}, \tag{3}$$

where V_{P0} and V_{S0} are the P and S velocities along the symmetry axis, respectively; ε, δ, and γ are the Thomsen parameters; ν and α are the tilt and azimuth of the symmetry axis, respectively. All of these parameters can be spatially varying and can be related directly to the stiffness tensor $c_{ijk\ell}$.

Mathematically, the separation is first carried out with reference model $\mathbf{m}^k$, $k = 1, 2, \ldots N$, with N being the number of reference models. Then the wave modes are inverse Fourier transformed to the space domain:

$$M^k(\mathbf{x}) = \mathcal{F}^{-1}\left\{\sum_{j=1}^{3} i\tilde{W}_j(\mathbf{k})U_{Mj}^k(\mathbf{k})\right\}. \tag{4}$$

Here, M stands for different wave modes, i.e., P, SV, and SH, and j stands for the x-, y-, and z-components of the wavefields, i.e., $j = 1, 2, 3$, and i is the imaginary unit. $\tilde{W}$ is the k-domain wavefield and $\mathcal{F}^{-1}\{\,\}$ denotes inverse Fourier transform. At a homogeneous reference model $\mathbf{m}^k$, the polarization vector components are expressed by

$$U_{Mj}^k = U_{Mj}\left(\mathbf{m}^k\right). \tag{5}$$

At any given heterogeneous model $\mathbf{m}(\mathbf{x})$, one can express its polarization vectors as a weighted sum of the vectors at a subset of the reference models:

$$U_{Mj}(\mathbf{m}(\mathbf{x})) = \sum_k w^k\left(\mathbf{m}(\mathbf{x}), \mathbf{m}^1, \mathbf{m}^2, \cdots, \mathbf{m}^N\right)U_{Mj}\left(\mathbf{m}^k\right). \tag{6}$$

A Fourier transform of Equation 6 gives the $\mathbf{x}$-domain weighted filters as

$$L_{Mj}(\mathbf{x}) = \sum_k w^k(\mathbf{x})L_{Mj}^k(\mathbf{x}). \tag{7}$$

Next, one can separate the wave modes for a heterogeneous model as a weighted sum of the wave modes obtained at the homogeneous reference models. From Equation A-2, an accurate P-mode separation in the space domain is formulated as

$$P = L_{Px}[W_x] + L_{Py}\left[W_y\right] + L_{Pz}[W_z], \tag{8}$$

where W_x, W_y, and W_z are the x, y, and z components of the elastic wavefields. Generally, for P, SV, or SH mode, this equation can be written as

$$M(\mathbf{x}) = \sum_{j=1}^{3} L_{Mj}(\mathbf{x})\left[W_j(\mathbf{x})\right], \tag{9}$$

where j denotes a Cartesian component in 3D. Insertion of Equation 7 into Equation 9 yields

$$M(\mathbf{x}) = \sum_{j=1}^{3} \left(\sum_{k} w^k(\mathbf{x}) L^k_{Mj}(\mathbf{x}) \right) \left[W_j(\mathbf{x}) \right]. \tag{10}$$

Rearranging this equation, we obtain

$$M(\mathbf{x}) = \sum_{k} w^k(\mathbf{x}) \left\{ \sum_{j=1}^{3} L^k_{Mj}(\mathbf{x}) \left[W_j(\mathbf{x}) \right] \right\}. \tag{11}$$

The term in the curly brackets is a separated mode using reference model $\mathbf{m}^k$ in Equation 9. Therefore, we have the interpolated wave modes as

$$M(\mathbf{x}) = \sum_{k} w^k(\mathbf{x}) M^k(\mathbf{x}). \tag{12}$$

Here, we see that the weights used to interpolate among the separated wave modes M^k (in Equation 12) are exactly the same as the weights used to interpolate among the polarization vectors U^k (in Equation 6) or space-domain filters L^k (in Equation 7). Therefore, one needs to compute the weights based on the heterogeneous multi-dimensional model, and then use these weights to obtain the interpolated wave modes.

The separation problem now becomes a question of how to find the interpolation weights for the chosen reference models. There are two methods one can use:

1) Determine the form of the function one wants to interpolate (the polarization vectors, in this case), use a few references to define the function (model), and then calculate the weights for the reference models based on the function. We call this process the "analytic" method.
2) Regardless of the form of the function, find the interpolation weights for the reference models using numerical interpolation methods, e.g., inverse-distance weight interpolation, natural neighbor interpolation, etc. For symmetry, we refer to this process as the "numerical" method.

In the following, we show the implementation of both methods and compare their performance.

ANALYTIC INTERPOLATION METHOD

This section describes the dependence of the polarization vectors on model parameters. From the approximate function form of the vectors, one can find the interpolation weights for the references at an arbitrary model.

In an anisotropic medium, the P-, SV-, and SH-modes are polarized orthogonal to each other for a fixed wave vector **k**, as depicted by Figure 1. The P- and SV-modes are polarized in the symmetry-axis plane, and the SH-mode is polarized in the isotropy plane. The P-mode polarization vector **P** deviates from the wave vector **k** by an angle Δ. From the illustration, one can see that the easiest to separate is the SH-mode because it is always polarized in the isotropy plane, and this fact is not influenced by the strength of anisotropy. From Equation A-10, we have

$$\begin{aligned} U_{SHx} &= k_z n_y - k_y n_z, \quad U_{SHy} = k_x n_z - k_z n_x, \\ U_{SHz} &= k_y n_x - k_x n_y. \end{aligned} \tag{13}$$

These equations show that the SH-mode polarization does not depend on anisotropy and that the mode can be interpolated between separated SH modes that are obtained using different symmetry axes **n**. Because only two variables (two **n** components) exist in each polarization vector component, only two references are needed for interpolation of all $\mathbf{U}_{SH}$ components:

$$U_{SHj}(\mathbf{n}) = \sum_{k=1}^{2} w^k U_{SHj}(\mathbf{n}^k). \tag{14}$$

For a heterogeneous TTI model, the SH-mode can be obtained by

$$SH(\mathbf{x}) = \sum_{k=1}^{2} w^k(\mathbf{x}) SH^k(\mathbf{x}), \tag{15}$$

where $SH^k = \mathcal{F}^{-1}\{\sum_{j=1}^{3} i\tilde{W}^k_j U^k_{SHj}\}$.

For VTI media, the P-wave polarization angle can be approximately represented by the expression (Tsvankin, 2005)

$$v_P = \theta + B\left[\delta + 2(\varepsilon - \delta)\sin^2\theta\right]\sin 2\theta, \tag{16}$$

with

$$B = \frac{1}{2\left(1 - V^2_{S0}/V^2_{P0}\right)}.$$

Here, V_{P0} and V_{S0} are P- and S-wave velocities along the symmetry axis; the angle θ is the angle between the phase vector **k** and the symmetry axis **n** (Figure 1). This expression is an approximation for weakly anisotropic media and indicates that the anisotropic polarization vector (**U**) deviates from the isotropic polarization vector (**k**) by a small angle Δ:

$$v_P = \theta + \Delta(\theta, B, \varepsilon, \delta). \tag{17}$$

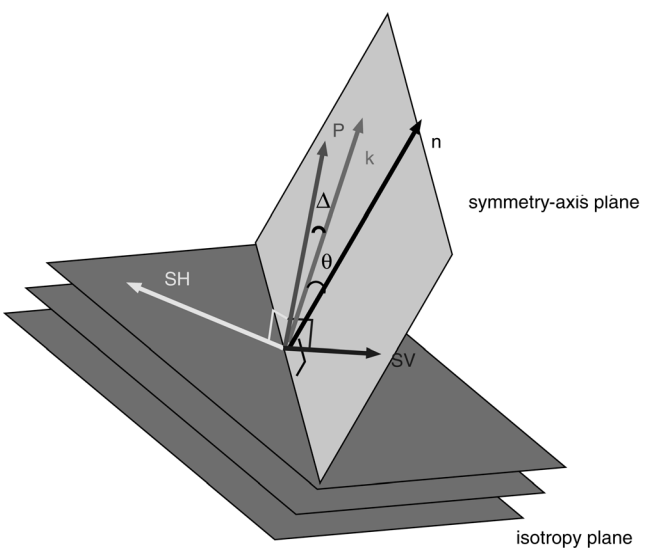

Figure 1. Schematic showing the elastic wave-mode polarization in a 3D TI medium. The three parallel planes represent the isotropy planes of the medium. The vector **n** represents the symmetry axis, which is orthogonal to the isotropy plane and has tilt angle ν and azimuth angle α. The vector **k** is the propagation direction of a plane wave. The angle between vectors **k** and **n** is the polar angle θ in Equation 16. Wave modes **P**, **SV**, and **SH** are polarized in the directions **P**, **SV**, and **SH**, respectively, and are polarized orthogonal to each other for a fixed wave vector **k**. The deviation of vectors **P** and **k** indicates that the medium is anisotropic.

For a 3D TTI medium, whose symmetry-axis tilt and azimuth angles are nonzero, the orientation of the P polarization vector also depends on these two angles. By making new variables $\varepsilon' = B\varepsilon$ and $\delta' = B\delta$ and assuming a small angle Δ, we get

$$\begin{aligned} U_{Mj} &= U^0_{Mj} + \Delta U_{Mj} \\ &\approx U^0_{Mj} + (a\varepsilon' + b\delta') \sum_{i\le j} \sum_{j=1}^{3} d_{ij} n_i n_j, \end{aligned} \tag{18}$$

where a, b, d_{ij} are functions of θ (refer to Appendix B for derivation). Here, M can be P or SV mode, and $n_i (i = 1, 2, 3)$ is a component of the symmetry axis **n**.

In summary, the analytic method finds the dependence of the polarization angles on the Thomsen parameters (ε and δ) and the symmetry-axis-related parameters (n_x, n_y, n_z or ν and α), and one can use the function for weights computation. The benefit of using this analytic method is that the choice of reference models is not critical because one can use the function to compute the weights for each reference model based on Equation 18. The shortcoming is that the polarization vector function we use is an approximation; thus the polarization vectors obtained at the reference models are not exact.

This section discusses the possibility of simplifying the dependence of the polarization vectors on various model parameters and using the model to calculate the interpolation weights. We discuss the numerical interpolation approach in the following section.

NUMERICAL INTERPOLATION METHOD

Besides the analytic interpolation approach, alternatively, one can find the interpolation weights using standard numerical interpolation methods for scattered data, such as inverse-distance weighting (IDW) and natural neighbor interpolation. Other interpolation methods usually require gridded data points and the number of data points grows rapidly with the increased dimension of the model space. For example, if one is satisfied with linear interpolation in 4D, then he has to use at least $2^4 = 16$ data points, because two points make a line in each dimension. If one wants to use polynomial or spline interpolation with degree higher than one, then at least $3^4 = 81$ data points have to be used for a 4D interpolation. In this section, we test with the IDW method, which is easiest to implement.

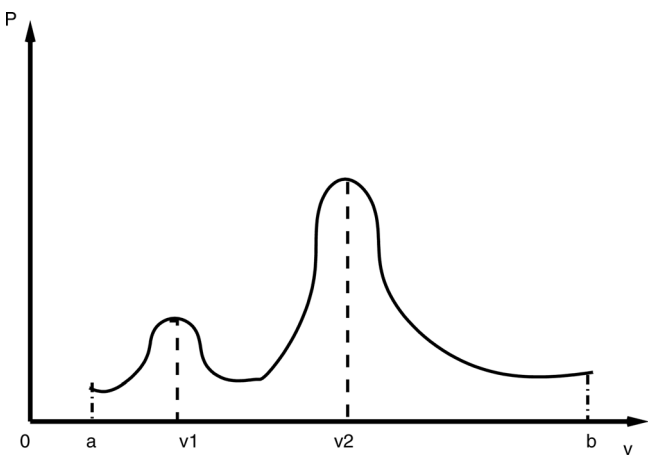

Figure 2. Illustration showing the distribution of a model parameter. The parameter (P-wave velocity, for example) spreads over the range (a, b), and the area under the curve is 1. Velocity v_1 and v_2 are picked as references because of their high occurrence frequency.

Even though the model space shown in Equation 3 is seven-dimensional, we show in the previous section that the γ parameter does not influence the mode polarization (even for the SH mode; see Equation 13) and we simplify the problem by making new variables $\varepsilon' = B\varepsilon$ and $\delta' = B\delta$.

Inverse distance weighting interpolation

Inverse distance weighting (IDW) is suitable for multivariate interpolation. The method assigns values to non-nodal points by using values from the usually scattered set of nodal points (Shepard, 1968). The value at a given model **m** is interpolated from N known reference models $\mathbf{m}^k$, k = 1…N:

$$U_{Mj} = \sum_{k=1}^{N} \frac{w^k}{\sum_{k=1}^{N} w^k} U^k_{Mj}, \tag{19}$$

where the weight

$$w^k = \frac{1}{\|\mathbf{m} - \mathbf{m}^k\|} \tag{20}$$

is inversely proportional to the distance of the model **m** to the known reference model $\mathbf{m}^k$. The normalization in the weights assures that the weights vary between 0 and 1 and the sum of all weights is 1. The advantage of using IDW interpolation is that it is simple to implement and extends straightforwardly to high dimensions. Therefore, it is applicable to 2D and 3D TTI wave-mode separation. A potential drawback is that the weights calculated using IDW might be not accurate enough for just a few scattered points in a large model space.

Reference model selection

In contrast to the analytic method, in numerical interpolation, the choice of reference models is critical. Because the model space is at least 4D for 3D TTI models, it is difficult to visualize the model space. Therefore, we use a method for high-dimensional reference-model picking extended from its 1D equivalent. As depicted in Figure 2, a model parameter of the medium can have a distribution similar to that shown by the curve. The horizontal axis is a model parameter (for instance, the P-wave velocity V) of the medium, and the vertical axis is the population density of this parameter. The parameter spreads over the range (a, b), the population density ranges from 0 to 1, and the area under the curve is 1. For this 1D problem, we first choose a threshold of occurrence frequency and assume that only velocities with higher occurrence frequency than this threshold are candidates for reference models. Then, we choose the reference models represented by the two peaks of the curve, which have the highest occurrence frequency over the entire model space. This crude method for picking reference velocities in 1D assumes that along the curve there is only one peak in a neighborhood. Otherwise many close reference models will be picked, which is wasteful for the following processing. Similarly, in high dimensions, we

first compute the population density of all model parameters, then we choose a threshold and find the local maximums as the reference models.

EXAMPLES

We illustrate the method presented in this paper with 2D and 3D examples. We start with a 2D benchmark test and an elastic version of 2D Marmousi II. The 3D examples include a 3D fold model and a 3D version of the elastic Marmousi II.

2D benchmark test

We illustrate the separation technique with a 2D benchmark test. In this example, we propagate elastic wave modes that are triggered by a vertical point force in a homogeneous TTI model. The model has parameters $V_{P0} = 3.0$ km/s, $V_{S0} = 1.5$ km/s, $\rho = 2.0$ g/cm^3, $\varepsilon = 0.3$, $\delta = 0.1$, $\gamma = 0.0$, and tilt angle $\nu = 30°$. The separation is achieved by mixed-domain separation with either numerical or analytic interpolation. We choose reference models that are not on the true model to test the interpolation error. The chosen reference models for both methods are shown in Figure 3. In each panel of Figure 3, the illustration depicts the model space $\{\varepsilon, \delta, \nu\}$. The dot in the model space represents the true model. For inverse distance weighting interpolation, we choose four (Figure 3a) or eight (Figure 3b) reference models that are equal "distance" away from the true model. Figure 3a shows four reference models that are at the correct tilt angle 30° and incorrect ε and δ (± 0.05 the true values), represented by the vertices of the square. Figure 3b shows eight reference models that are at incorrect tilt angles ($\pm 10°$ the true value) and incorrect ε and δ (± 0.05 the true values), represented by the vertices of the cube. For analytic interpolation, Figure 3c shows nine reference models that are the nine vertices of the three triangles (errors in ε and δ are ± 0.05 and the error in tilt angle is $\pm 10°$). Figure 4 is a snapshot of the elastic wavefield. Figure 5a and 5b is the separated modes using inverse distance weighting interpolation with four and eight reference models, respectively. Figure 5c shows the separated modes using analytic interpolation. The results show that using inverse distance weighting and with correct tilt angle, the separation is very clean. If we further

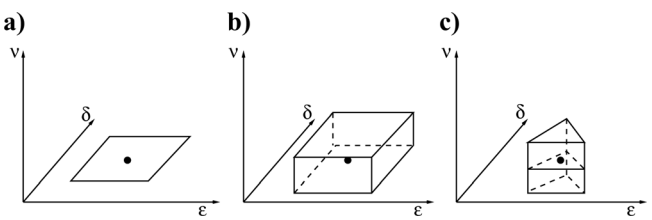

Figure 3. Illustration showing true model and reference models used for wave-mode separation in a 2D benchmark test example. The 3D coordinate system shows model space $\{\varepsilon, \delta, \nu\}$. The dot denotes the true model. Panels (a) and (b) show references used for inverse-distance weighting interpolation, and they used four and eight reference models, respectively, where the vertices are the reference models. Panel (c) shows reference models for analytic interpolation, where a total number of nine reference models are used.

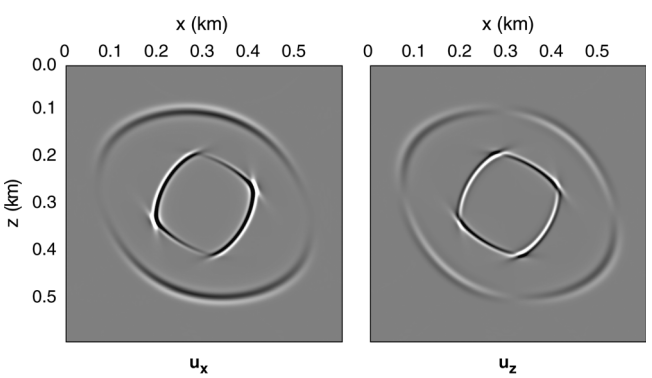

Figure 4. A snapshot of the elastic wavefield in the vertical (left) and horizontal (right) direction for a homogeneous TTI model. The model has parameters $V_{P0} = 3.0$ km/s, $V_{S0} = 1.5$ km/s, $\rho = 2.0$ g/cm^3, $\varepsilon = 0.3$, $\delta = 0.1$, $\gamma = 0.0$, and tilt angle $\nu = 30°$.

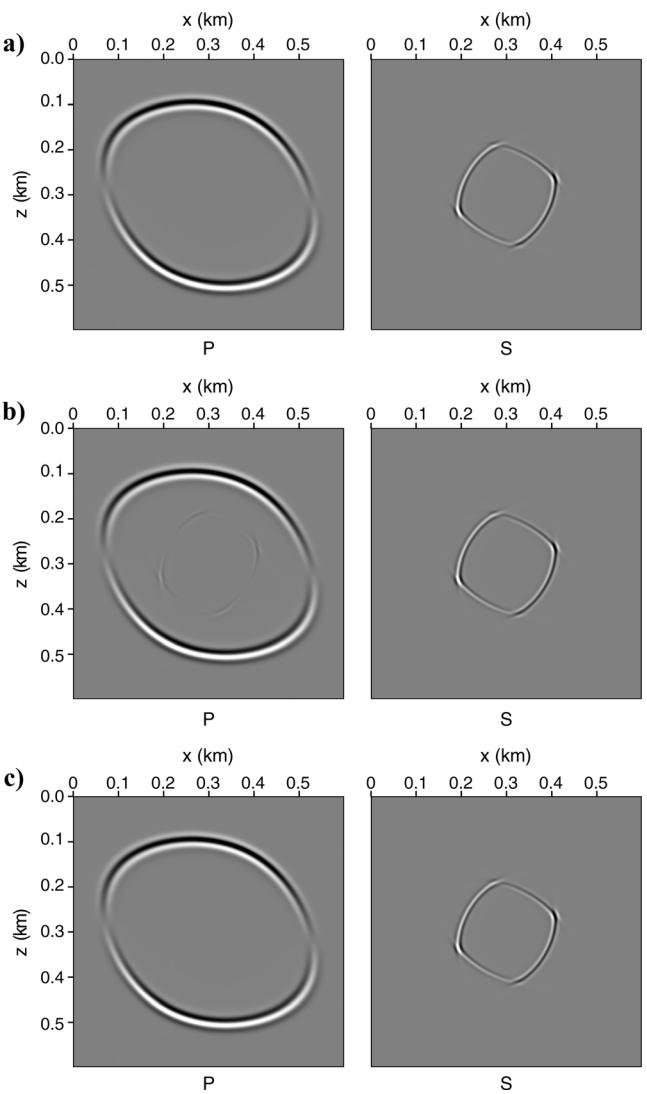

Figure 5. Separated P (left) and S (right) modes using inverse-distance weighting interpolation (a and b) and analytic interpolation (c). The reference models are chosen according to the cartoons shown in Figure 3a, 3b, and 3c, respectively.

allow the error in the tilt angle, then the separation is noisier and more leakage of shear mode is visible in the P panel. The separation using the nine reference models shown in Figure 5c yields very clean separation. In this test we intentionally choose reference models so that IDW assigns equal weights to all reference models. If given correct tilt angles, the IDW interpolation yields clean separation (Figure 5a), showing a linear relationship of polarization angles and ε and δ. Figure 5b verifies a nonlinear relationship between polarization angles and the tilt v. The analytic separation shown in Figure 5c also validates the derived Equation 18.

2D Marmousi model

We use a 2D Marmousi model to test the feasibility of the mixed-domain separation. Figure 6a, 6b, 6c, and 6d shows model parameters V_{P0}, ε, δ, and tilt angle v, respectively. Figure 7 shows the variation of the parameters ε, δ, and tilt angle v in the model space. A visual examination reveals that there are three clouds in the model space, and the reference selection algorithm based on population density chooses 15 references out of the three clouds (of course, the number of picked references changes with different choice of threshold). These 15 references are used for the numerical interpolation. Figure 8 is a snapshot

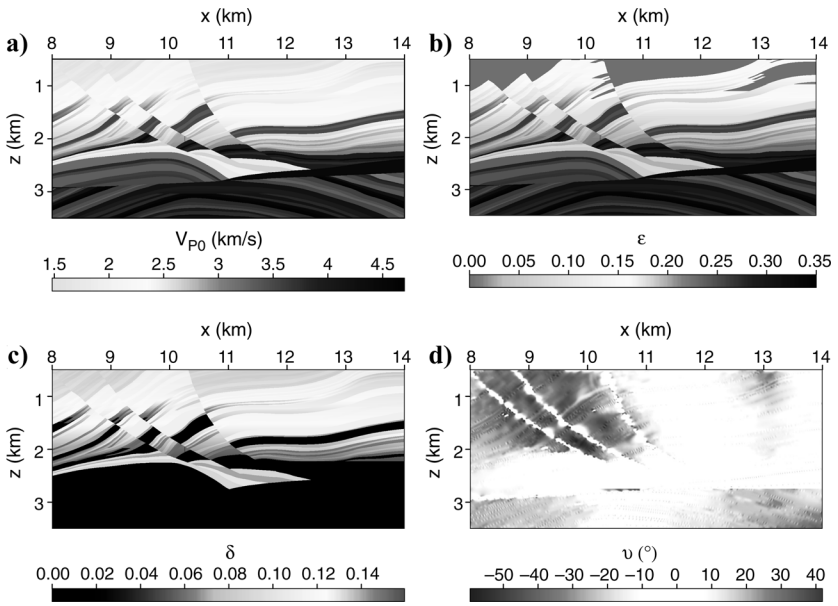

Figure 6. Model parameters of a 2D elastic Marmousi II model showing varying (a) V_{P0}, (b) ε, (c) δ, and (d) tilt angle v.

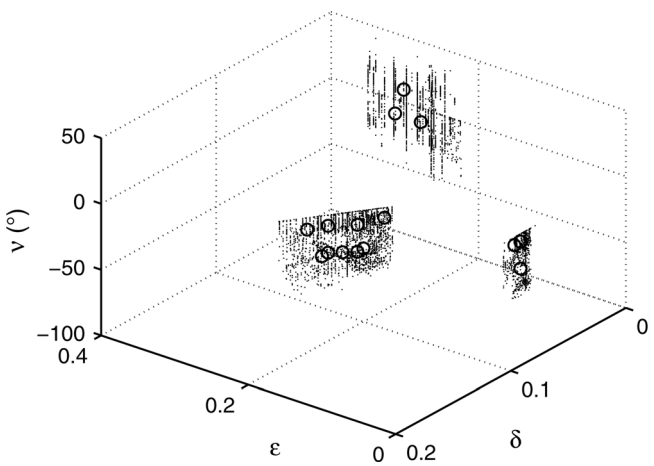

Figure 7. Model space showing the variation of the parameters ε, δ, and tilt angle v for the model shown in Figure 6. Each dot represents the occurrence of one combination of (ε, δ, v) in the physical model. The dots form three clouds in this space. The circles are the computed reference models, which are selected based on the criterion depicted in Figure 2.

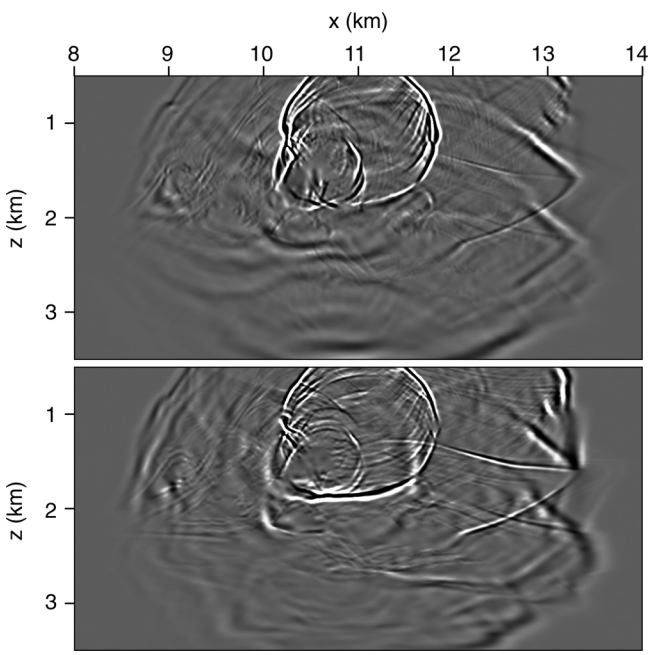

Figure 8. A snapshot of the elastic wavefields in vertical and horizontal directions for the model shown in Figure 6.

of the elastic wavefields in the z (top) and x (bottom) direction. Figure 9a and 9b shows the wave-mode separation using the analytic procedure and IDW, respectively. A comparison of the separation results indicates that all the methods can separate P and S modes. Among them, the analytic method obtains the cleaner P separation at the top of the model. IDW interpolation achieves similarly good separation results, while exhibiting some visible residual at the top of the model in the P panel, for example at $x = 11.5$ km and $z = 1.0$ km. This artifact suggests that the selected references do not represent the model parameters in that region and that a better reference selection algorithm might be needed. This result is also consistent with the benchmark test, which suggests that a denser sampling in tilt angle is probably necessary.

3D fold model

The first 3D wave-mode separation example uses a fold model with spatially varying ε and δ. The model has a constant V_{P0}/V_{S0} ratio equal to two and $\gamma = 0.0$. The symmetry axis is perpendicular to the layering throughout the model. Figure 10 shows the spatially varying ε, δ, tilt ν, and azimuth α. The 3D model has a size of 480 m^3. To simulate elastic wavefields, we mesh the model with a sampling interval of 2 m and use a point force in the direction given by a vector with components $\{1, 1, 1\}$. Figure 11 is a snapshot of the elastic wavefields. Figure 12a and 12b shows the separation with the analytic method and IDW interpolation, respectively. Here, we show only the separated P mode for clarity. A comparison shows that the analytic method obtains a cleaner separation. However, both methods have some residual because the tilt and azimuth of the model

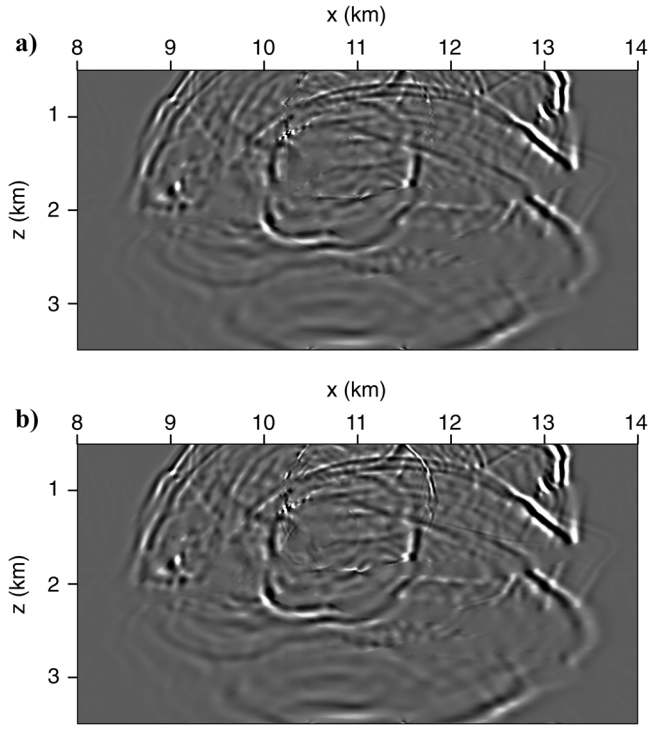

Figure 9. Mode separation of P-mode using (a) the analytic method and (b) inverse distance weighting interpolation for elastic wavefields shown in Figure 8. To show the residual clearly, we only show the separated P mode.

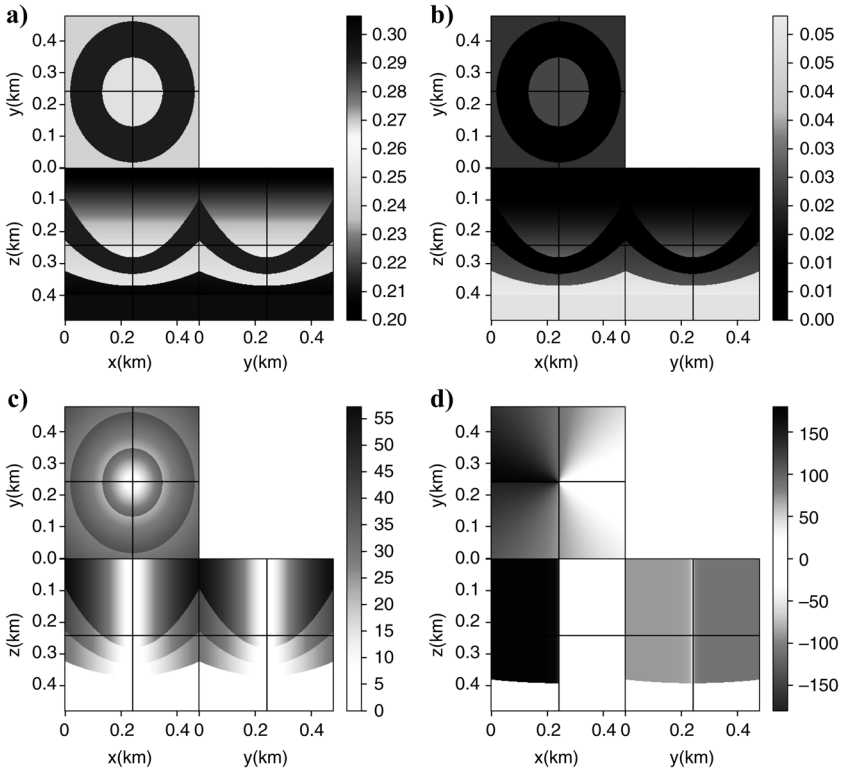

Figure 10. Three-dimensional TTI fold with model parameters (a) ε, (b) δ, (c) tilt angle ν, and (d) azimuth angle α.

have wide ranges, and the chosen reference cannot well represent the model in this extreme case.

3D Marmousi model

The last example is a 3D version of the elastic Marmousi model. The first vertical slices of V_{P0}, V_{S0}, and density are taken from the original 2D model. In the y-direction, the vertical slice is shifted constantly to make the next vertical slice. This ensures that the medium has a constant azimuth angle (26°) of anisotropy symmetry axis. The 3D model has a size of 1280 m^3. To simulate elastic wavefields, we mesh the model with a sampling interval of 5 m and use a point force in the direction given by a vector with components $\{1, 1, 1\}$. Thomsen parameters are derived from the velocity and density model with the relationship of $\varepsilon = 0.5\rho/max(\rho)$ and $\delta = 0.25V_{P0}/max(V_{P0})$. Figure 13a, 13b, 13c, and 13d shows V_{P0}, ε, δ, and tilt angle v of the 3D model, respectively. Figure 14 shows the variation of the parameters ε, δ, and tilt angle v in the model space. The circles are the computed reference models, which are selected based on the criterion depicted in Figure 2. Figure 15 shows a snapshot of the elastic wavefields. Figure 16a and 16b shows separation using analytic and IDW methods, respectively. Here, we show only the separated P mode for clarity. Both methods obtain

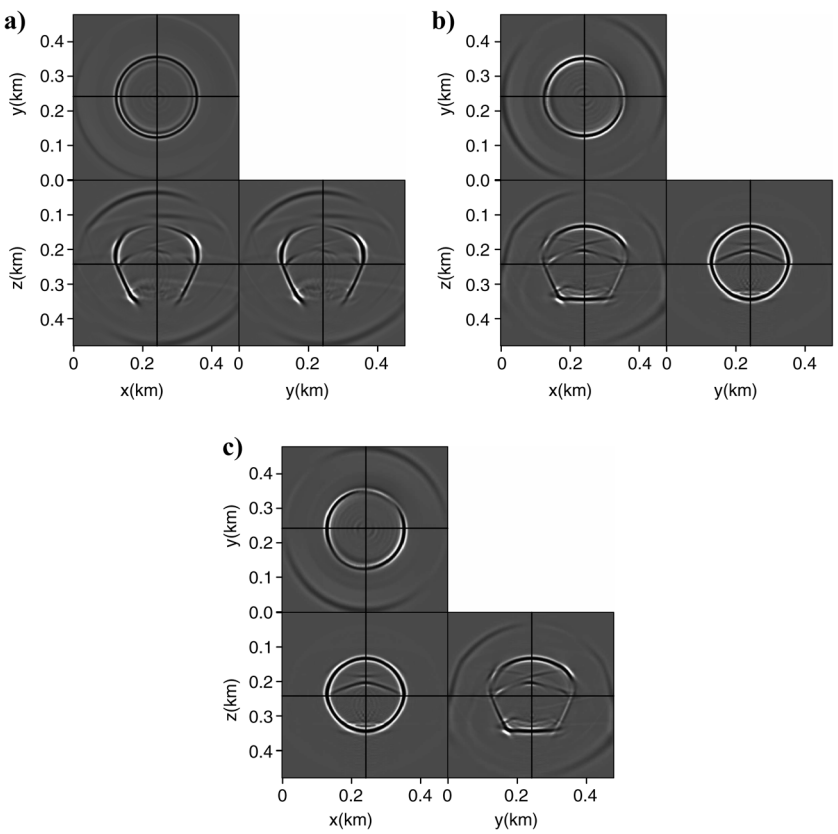

Figure 11. (a) A snapshot of the elastic wavefields in the z (left), x (middle), and y (right) directions for the model shown in Figure 10.

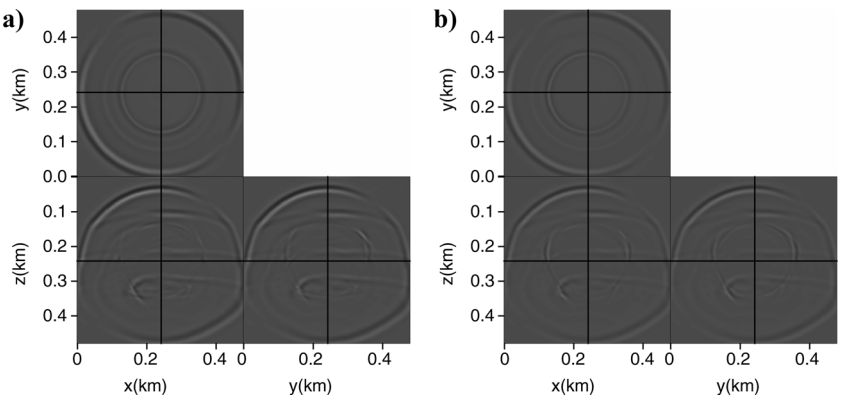

Figure 12. Separated P mode using (a) the analytic methods and (b) inverse-distance weighting interpolation for elastic wavefields shown in Figure 11. To show the residual clearly, we only show the separated P mode.

good separation results. The successfully separated modes obtained with IDW interpolation suggest that the selected models represent the entire model space well.

DISCUSSION

As was demonstrated by the synthetic examples, the separation in the space domain by nonstationary filtering is accurate but computationally expensive; meanwhile, the separation in the mixed domain is less accurate but much cheaper. The cost of separation in the space domain is proportional to the model size times the size of the separators, which becomes prohibitive in 3D. In comparison, the cost of separation in the mixed domain is just proportional to the number of used references, which includes wavefield projection and Fourier transforms of the wavefields.

In the analytic procedure, the interpolation error comes from the approximate representation of the dependence of the polarization angles on ε, δ, tilt ν, and azimuth α (Equation 18). Strictly speaking, the anisotropic polarization vector is only approximately represented by Equation 18 in 3D. However, the synthetic examples show that mode separation is effective in the mixed domain with the analytic procedure, which suggests that for weak anisotropy, the polarization vector function we used does not deviate much from the true vector directions.

In the numerical interpolation procedure, to decrease the dimensionality for interpolation, we assume that some model parameters are interrelated. For example, we draw upon the fact that the Thomsen parameter γ does not play a role in the polarization of wave modes. We also learn from Equation 16 that it is the ratio of V_{P0} and V_{S0} that affects the polarization vectors and that they do not affect the function independently, so we make new variables $\varepsilon' = \varepsilon$ and $\delta' = B\delta$. These observations help one to decrease the dimensionality of the interpolation problem. For the numerical approach, the separation accuracy increases with the number of reference models one uses. However, to limit the cost of separation, one should try to use fewer reference models, which might increase interpolation error.

The reference model selection is necessary in both approaches. Because we use a function to compute the weights in the analytic procedure, the locations of the reference models are not really important. In comparison, for the numerical approach, the reference models should represent the model space of the medium for the best interpolation results. Therefore, the analytic approach is more deterministic, while the numerical approach is more stochastic. To obtain better separation results with the numerical approach, one needs to determine the reference models that best represent the model space, and the choice of the models is case dependent.

In summary, both analytic and numerical methods can have interpolation errors. The inverse distance weighting interpolation method is easy to understand and particularly easy to implement with inverse-distance weighting interpolation. In the 2D tests, the analytic method yields cleaner separation, but in 3D the approximate equation we use as the underlying "true" function also subjects the separation to errors when the model parameters have a large range.

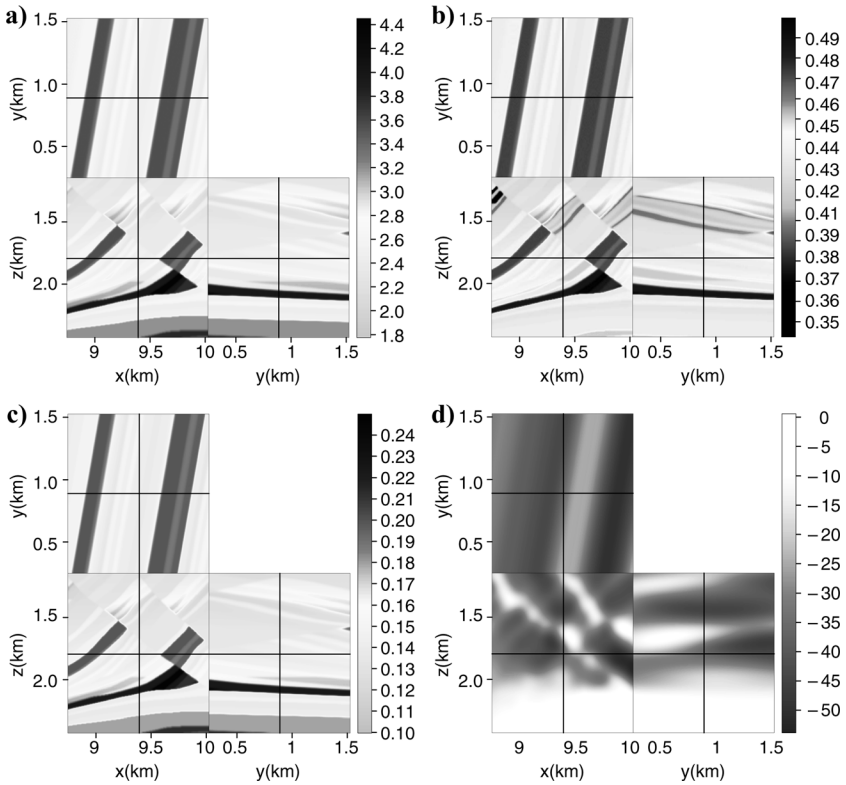

Figure 13. Three-dimensional Marmousi model with model parameters (a) V_{P0}, (b) ε, (c) δ, (d) tilt angle ν.

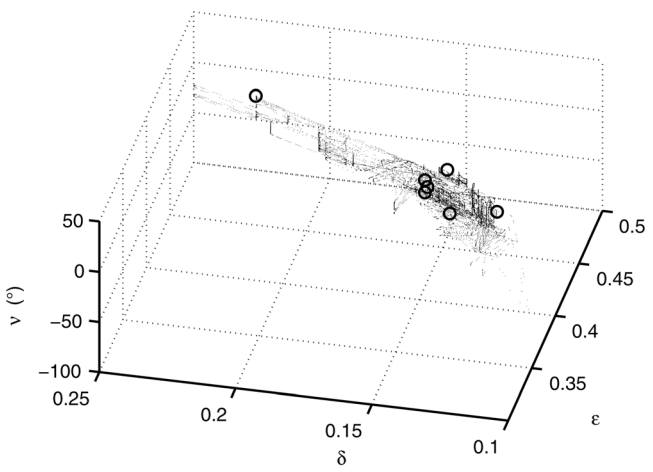

Figure 14. Model space showing the variation of the parameters ε, δ, and tilt angle ν for the models shown in Figure 13. Each dot represents the occurrence of one combination of $(\varepsilon, \delta, \nu)$ in the physical model. The dots are widely spread in this space. The circles are the computed reference models, which are selected based on the criterion depicted in Figure 2.

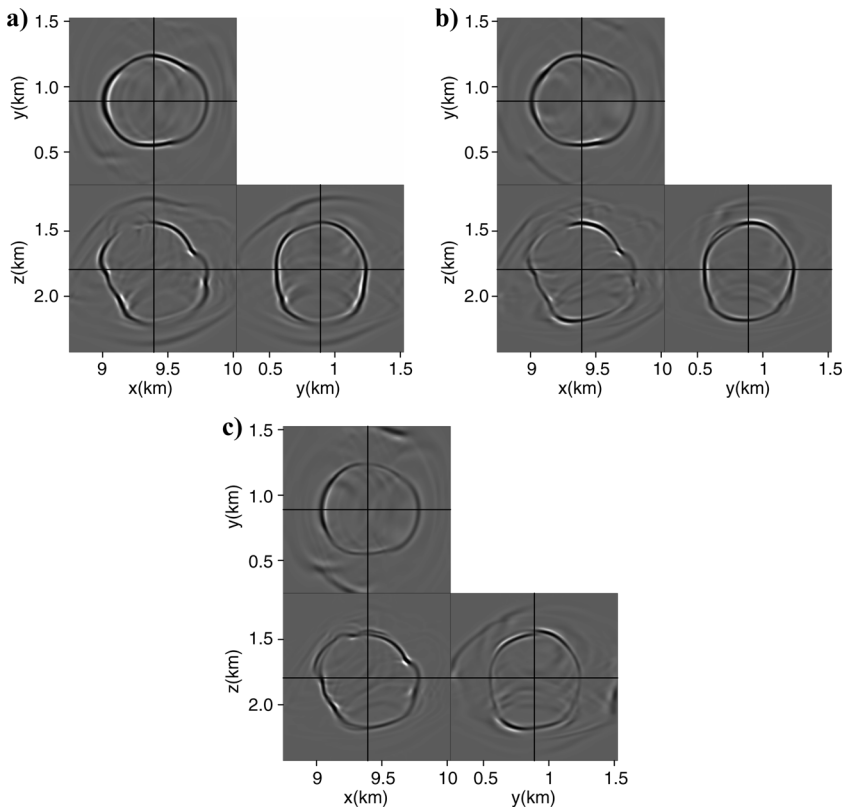

Figure 15. (a) A snapshot of the elastic wavefields in the z (left), x (middle), and y (right) directions for the model shown in Figure 13.

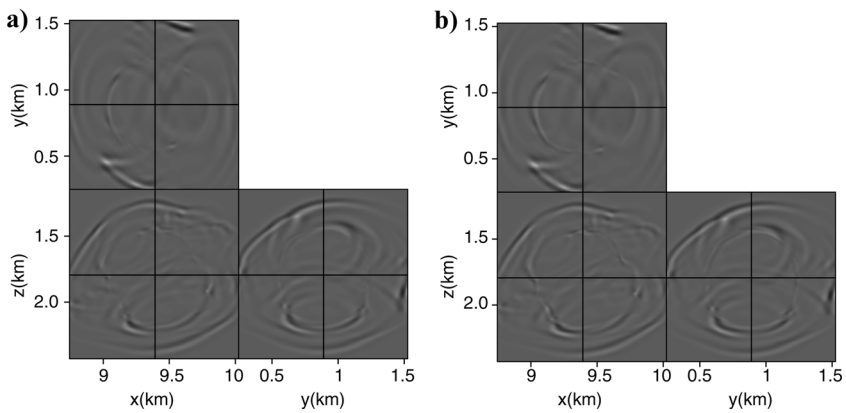

Figure 16. Separated P mode using (a) the analytic methods and (b) inverse-distance weighting interpolation for elastic wavefields shown in Figure 15. To show the residual clearly, we only show the separated P mode.

CONCLUSIONS

We present a mixed-domain wave-mode separation method applicable to complex media. First, we separate wave modes in the wavenumber domain at different reference values of the anisotropy parameters ε, δ, tilt angle ν, and azimuth angle α. This is followed by interpolation in the space domain. We test two separation schemes. One of them derives a relatively simple function of the polarization vectors; we then use this function to compute the interpolation weights. The other is designed to compute the interpolation weights numerically with various interpolation methods. Although the space-domain nonstationary filtering is more accurate for heterogeneous media, it is very expensive. In comparison, the separation in the mixed domain has the advantage of being much more computationally efficient. The mixed-domain separation is especially beneficial for 3D models because the space-domain separation is prohibitively expensive. We test the mixed-domain separation method with several synthetic examples and show that both separation schemes are computationally feasible and effective.

ACKNOWLEDGMENTS

We acknowledge the support of the sponsors of the Center for Wave Phenomena at Colorado School of Mines. The authors are grateful to the associate editors and all reviewers whose constructive comments helped to improve the manuscript tremendously.

APPENDIX A

WAVE-MODE SEPARATION IN THE SPACE DOMAIN

For homogeneous models, the P mode can always be achieved by projecting the elastic wavefields onto the P-wave polarization vectors in the wavenumber domain (Dellinger and Etgen, 1990; Dellinger, 1991):

$$\tilde{P} = i\mathbf{U}_P(\mathbf{k}) \cdot \tilde{W} = iU_{Px}\tilde{W}_x + iU_{Py}\tilde{W}_y + iU_{Pz}\tilde{W}_z, \quad \text{(A-1)}$$

where $\tilde{P}$ is the P mode in the wavenumber domain, $i = \sqrt{-1}$, $\mathbf{k} = \{k_x, k_y, k_z\}$ is the wave vector, $\tilde{W}$ is the elastic wavefield in the wavenumber domain, and $\mathbf{U}_P(\mathbf{k})$ is the P-wave polarization vector as a function of $\mathbf{k}$.

For heterogeneous models, P mode can be obtained in the space domain by carrying out nonstationary filtering in the model:

$$P = L_{Px}[W_x] + L_{Py}[W_y] + L_{Pz}[W_z], \quad \text{(A-2)}$$

where L_{Px}, L_{Py}, and L_{Pz} represent the inverse Fourier transforms of iU_{Px}, iU_{Py}, and iU_{Pz}, respectively; L defines the "pseudo-derivative operators" (Yan and Sava, 2009b). These operators can change spatially according to the material parameters. Here, $[\cdot]$ represents spatial filtering of the wavefield with anisotropic operators.

The P-wave polarization vectors $\mathbf{U}_P = \{U_{Px}, U_{Py}, U_{Pz}\}$ can be calculated by solving the 3D Christoffel equation (Aki and Richards, 2002; Tsvankin, 2005):

$$\begin{bmatrix} G_{11} - \rho V^2 & G_{12} & G_{13} \\ G_{12} & G_{22} - \rho V^2 & G_{23} \\ G_{13} & G_{23} & G_{33} - \rho V^2 \end{bmatrix} \begin{bmatrix} U_{Px} \\ U_{Py} \\ U_{Pz} \end{bmatrix} = 0, \quad \text{(A-3)}$$

where $\mathbf{G}$ is the Christoffel matrix with $G_{ij} = c_{ijk\ell}\hat{k}_j\hat{k}_\ell$, in which $c_{ijk\ell}$ is the stiffness tensor. The vector $\hat{\mathbf{k}} = \frac{\mathbf{k}}{|\mathbf{k}|}$ is the unit vector orthogonal to the plane wavefront, with $\hat{k}_j$ and $\hat{k}_\ell$ being its components in the j and ℓ directions. Here, the subscripts $i, j, k, \ell = 1, 2, 3$ represent a Cartesian coordinate system. The eigenvalues V of this system correspond to the phase velocities of different wave modes and are dependent on the plane wave propagation direction $\mathbf{k}$.

For TTI media, the matrix $\mathbf{G}$ has the following elements:

$$G_{11} = c_{11}\hat{k}_1^2 + c_{66}\hat{k}_2^2 + c_{55}\hat{k}_3^2 + 2c_{16}\hat{k}_1\hat{k}_2 + 2c_{15}\hat{k}_1\hat{k}_3 + 2c_{56}\hat{k}_2\hat{k}_3, \quad \text{(A-4)}$$

$$G_{22} = c_{66}\hat{k}_1^2 + c_{22}\hat{k}_2^2 + c_{44}\hat{k}_3^2 + 2c_{26}\hat{k}_1\hat{k}_2 + 2c_{46}\hat{k}_1\hat{k}_3 + 2c_{24}\hat{k}_2\hat{k}_3, \quad \text{(A-5)}$$

$$G_{33} = c_{55}\hat{k}_1^2 + c_{44}\hat{k}_2^2 + c_{33}\hat{k}_3^2 + 2c_{45}\hat{k}_1\hat{k}_2 + 2c_{35}\hat{k}_1\hat{k}_3 + 2c_{34}\hat{k}_2\hat{k}_3, \quad \text{(A-6)}$$

$$G_{12} = c_{16}\hat{k}_1^2 + c_{26}\hat{k}_2^2 + c_{45}\hat{k}_3^2 + (c_{12} + c_{66})\hat{k}_1\hat{k}_2 + (c_{14} + c_{56})\hat{k}_1\hat{k}_3 + (c_{25} + c_{46})\hat{k}_2\hat{k}_3, \quad \text{(A-7)}$$

$$G_{13} = c_{15}\hat{k}_1^2 + c_{46}\hat{k}_2^2 + c_{35}\hat{k}_3^2 + (c_{14} + c_{56})\hat{k}_1\hat{k}_2 + (c_{13} + c_{55})\hat{k}_1\hat{k}_3 + (c_{36} + c_{45})\hat{k}_2\hat{k}_3, \quad \text{(A-8)}$$

$$G_{23} = c_{56}\hat{k}_1^2 + c_{24}\hat{k}_2^2 + c_{34}\hat{k}_3^2 + (c_{25} + c_{46})\hat{k}_1\hat{k}_2 + (c_{36} + c_{45})\hat{k}_1\hat{k}_3 + (c_{23} + c_{44})\hat{k}_2\hat{k}_3. \quad \text{(A-9)}$$

Here, Voigt notation is applied to simplify notation: $c_{ijk\ell}$ is expressed as a 6×6 matrix c_{mn} with $ij \to m$ and $kl \to n$. Explicitly, we have $11 \to 1$, $22 \to 2$, $33 \to 3$, $23 \to 4$, $31 \to 5$, and $12 \to 6$ (Aki and Richards, 2002; Tsvankin, 2005).

In the vertical symmetry-axis planes of 2D TTI media, the SV-mode is polarized orthogonal to the P-mode; therefore, for a P-wave polarized in the direction $\{U_{Px}, U_{Pz}\}$, the SV-wave is polarized in the direction $\{-U_{Pz}, U_{Px}\}$.

In 3D TTI media, Yan and Sava (2009a) define SH- and SV-polarization relative to the P-wave in the following way:

$$\mathbf{U}_{SH} = \mathbf{n} \times \mathbf{k} = \{k_z n_y - k_y n_z, k_x n_z - k_z n_x, k_y n_x - k_x n_y\}, \quad \text{(A-10)}$$

and

$$\begin{aligned} \mathbf{U}_{SV} &= \mathbf{U}_P \times \mathbf{U}_{SH}, \\ &= \{k_y n_x U_{Py} - k_x n_y U_{Py} + k_z n_x U_{Pz} - k_x n_z U_{Pz}, \\ &\quad k_z n_y U_{Pz} - k_y n_z U_{Pz} + k_x n_y U_{Px} - k_y n_x U_{Px}, \\ &\quad k_x n_z U_{Px} - k_z n_x U_{Px} + k_y n_z U_{Py} - k_z n_y U_{Py}\}. \end{aligned} \quad \text{(A-11)}$$

Here, the symmetry axis vector $\mathbf{n} = \{\sin v \cos\alpha, \sin v \sin\alpha, \cos v\}$, where v and α are the tilt and azimuth of the symmetry axis. The wave vector $\mathbf{k}$ represents the plane wave propagation direction. Vectors $\mathbf{U}_P$, $\mathbf{U}_{SV}$, and $\mathbf{U}_{SH}$ are the P-, SV-, and SH-wave polarization vectors, respectively. The polarization vectors of all modes constructed in this way have smooth variation of magnitudes and directions in the wavenumber domain; therefore, they can be transformed to the space domain to become spatially-varying filters (Yan and Sava, 2009a). This definition of the shear-wave polarization vectors has zero amplitudes in the singular directions; therefore, only kinematically separates shear modes away from each other.

APPENDIX B

LINEAR APPROXIMATION FOR POLARIZATION VECTORS

The polarization vectors for 2D TTI media

For VTI media, the P-wave polarization angle can be approximately represented by the expression (Tsvankin, 2005)

$$v_P = \theta + B[\delta + 2(\varepsilon - \delta)\sin^2\theta]\sin 2\theta, \quad \text{(B-1)}$$

with

$$B = \frac{1}{2(1 - V_{S0}^2/V_{P0}^2)}.$$

Here, V_{P0} and V_{S0} are the P- and S-wave velocities along the symmetry axis; and the angle θ is the angle between the phase vector $\mathbf{k}$ and the symmetry axis $\mathbf{n}$ (Figure 1).

For a TTI medium with a nonzero tilt angle, equation B-1 takes the form

$$v_P = \theta + B[\delta + 2(\varepsilon - \delta)\sin^2(\theta - v)]\sin 2(\theta - v). \quad \text{(B-2)}$$

Here, the angle θ is the angle between the vector $\mathbf{k}$ and the vertical axis k_z. The angle $\theta - v$ gives the polar angle for the TTI medium. The anisotropic P-wave polarization vector ($\mathbf{U}$) deviates from the isotropic polarization vector ($\mathbf{k}$) by an angle Δ:

$$v_P = \theta + \Delta(\theta, \varepsilon', \delta', v), \tag{B-3}$$

where $\varepsilon' = B\varepsilon$ and $\delta' = B\delta$. The magnitude of the angle Δ is small. This is verified by Figure B-1a and B-1b, and Figure B-2a, which show that with moderate anisotropy ($\varepsilon = 0.4$, $\delta = 0.2$, and $V_{P0}/V_{S0} = 2$), and various tilt angles v, the angle Δ is no more than 0.25 radians (small enough for the following approximation).

Assuming small Δ, one can expand the P-wave polarization components into

$$\begin{aligned} U_{Px} &= \sin(\theta + \Delta) = \sin\theta\cos\Delta + \cos\theta\sin\Delta \\ &\approx \sin\theta + \cos\theta\Delta = k_x + k_z\Delta, \end{aligned} \tag{B-4}$$

$$\begin{aligned} U_{Pz} &= \cos(\theta + \Delta) = \cos\theta\cos\Delta - \sin\theta\sin\Delta \\ &\approx \cos\theta - \sin\theta\Delta = k_z - k_x\Delta. \end{aligned} \tag{B-5}$$

Figure B-1a and B-1b and equation B-1 show that the deviation angle is approximately linearly dependent on the anisotropy parameters ε' and δ'.

Figure B-2a shows that Δ does not linearly depend on v for fix ε and δ; however, one can try to fit the curves of Δ at different v with a scaled function of $\sin 2(\theta - v)$, shown by Figure B-2b. The fit is not exact due to the second term in the square bracket in equation B-2, which depends on θ. Thus, Δ is only approximately proportional to

$$\sin 2(\theta - v) = \sin(2\theta)\cos(2v) - \cos(2\theta)\sin(2v). \tag{B-6}$$

We can now write the second terms of equations B-4 and B-5 for 2D TI media in the form

$$\Delta U_{Mj} \approx (a\varepsilon' + b\delta')(c\cos 2v + d\sin 2v), \tag{B-7}$$

where a, b, c, and d are functions of k_x and k_z (or functions of θ).

At any model parameter $\mathbf{m} = \{\varepsilon, \delta, v\}$, we have the polarization vector

$$U_{Mj} = U^0_{Mj} + \Delta U_{Mj} = U^0_{Mj} + \sum_{k=1}^{N} w^k \Delta U^k_{Mj}. \tag{B-8}$$

For P mode, $M = P$, $U_{Px} = k_x$, and $U_{Pz} = k_z$. For SV mode, $M = SV$, $U_{SVx} = -k_z$, and $U_{SVz} = k_x$. The P or SV wave is obtained with

$$\begin{aligned} M &= \mathcal{F}^{-1}\left\{\sum_{j=1}^{2} iU_{Mj}\tilde{W}_j\right\} \\ &= \mathcal{F}^{-1}\left\{\sum_{j=1}^{2}\left[i\tilde{W}_j\left(U^0_{Mj} + \sum_{k=1}^{N} w^k\Delta^k\right)\right]\right\} \\ &= M^0 + \sum_{j=1}^{2}\sum_{k=1}^{N} w^k\mathcal{F}^{-1}\left\{i\tilde{W}_j\left(U^k_{Mj} - U^0_{Mj}\right)\right\} \\ &= M^0 + \sum_{k=1}^{N}\left(w^kM^k - w^kM^0\right) \\ &= \left(1 - \sum_{k=1}^{N} w^k\right)M^0 + \sum_{k=1}^{N}\left(w^kM^k\right) \\ &= \sum_{k=0}^{N} w^kM^k, \end{aligned} \tag{B-9}$$

where $M^0 = \mathcal{F}^{-1}\{\sum_{j=1}^{2} i\tilde{W}_jU^0_{Mj}\}$ is the separation with $\varepsilon = 0$ and $\delta = 0$ and $M^k = \mathcal{F}^{-1}\{\sum_{j=1}^{2} i\tilde{W}_jU^k_{Mj}\}$ is the separation with reference model at reference model $\mathbf{m}^k = \{\varepsilon^k, \delta^k, v^k\}$.

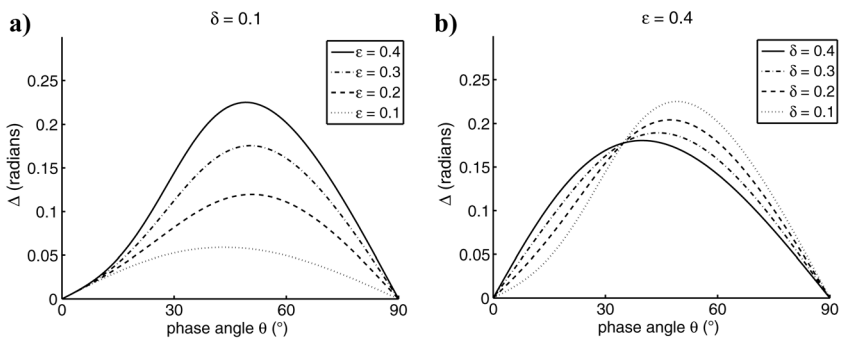

Figure B-1. Deviation angle of P-mode polarization from the wave vector $\mathbf{k}$ for VTI media with different combinations of ε and δ. (a) The deviation angle for parameter ε ranging from 0.1 to 0.4 and a fixed $\delta = 0.1$; (b) The deviation angle for parameter δ ranging from 0.1 to 0.4 and a fixed $\varepsilon = 0.4$. The deviation angles are approximately linearly dependent on ε and δ, which is consistent with the linearized equation B-1.

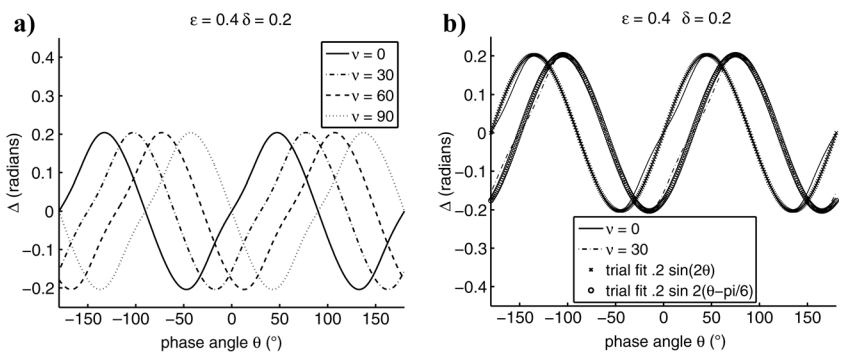

Figure B-2. Deviation angle of P-mode polarization from the wave vector $\mathbf{k}$ for TTI media ($\varepsilon = 0.4$, $\delta = 0.2$) with varying tilt angle v. (a) is the deviation angles for tilt angles 0, 30°, 60°, and 90°. The curves for these angles are a simple shift from each other by the angle v. (b) The deviation angle Δ can be approximated fit by a scaled function of $\sin 2(\theta - v)$.

The polarization vectors for 3D TTI media

The P-mode polarization vector $\mathbf{U}_P = \{U_{Px}, U_{Py}, U_{Pz}\}$ is always polarized in symmetry-axis planes, the planes formed by symmetry axis vector $\mathbf{n}$ and wave vector $\mathbf{k}$ at different directions. The P-mode polarization $\mathbf{U}_P$ can be obtained by rotating from $\mathbf{k}$ by a small deviation angle Δ (which is defined earlier for 2D) in the symmetry-axis plane (Figure 1):

$$\mathbf{U}_P = \mathbf{R}(\mathbf{u})\mathbf{k}, \tag{B-10}$$

where $\mathbf{R}(\mathbf{u})$ is the rotation matrix with a rotation axis $\mathbf{u} = \frac{\mathbf{n}\times\mathbf{k}}{|\mathbf{n}\times\mathbf{k}|}$ and rotation angle Δ. Letting $\mathbf{u} = \frac{\mathbf{n}\times\mathbf{k}}{|\mathbf{n}\times\mathbf{k}|} = \{x, y, z\}$ and assuming small Δ, one can express the rotation matrix as

$$\begin{aligned}\mathbf{R} &= \begin{pmatrix} 0 & -z & y \\ z & 0 & -x \\ -y & x & 0 \end{pmatrix}\sin\Delta + \left(\mathbf{I} - \mathbf{u}\mathbf{u}^T\right)\cos\Delta + \mathbf{u}\mathbf{u}^T \\ &\approx \begin{pmatrix} 0 & -z & y \\ z & 0 & -x \\ -y & x & 0 \end{pmatrix}\Delta + \mathbf{I} \\ &= \begin{pmatrix} 1 & -z\Delta & y\Delta \\ z\Delta & 1 & -x\Delta \\ -y\Delta & x\Delta & 1 \end{pmatrix},\end{aligned} \tag{B-11}$$

with $\cos\Delta \approx 1$ and $\sin\Delta \approx \Delta$. Substitution of Equation B-11 into Equation B-10 yields

$$\begin{aligned}&U_{Px} = k_x - zk_y\Delta + yk_z\Delta, \quad U_{Py} = k_y - xk_z\Delta + zk_x\Delta, \\ &U_{Pz} = k_z - yk_x\Delta + xk_y\Delta.\end{aligned} \tag{B-12}$$

We use U_{Px} as an example to expand Equation B-12:

$$\begin{aligned}U_{Px} &= k_x - zk_y\Delta + yk_z\Delta \\ &= k_x - \frac{(\mathbf{n}\times\mathbf{k})_z}{|\mathbf{n}\times\mathbf{k}|}k_y\Delta + \frac{(\mathbf{n}\times\mathbf{k})_y}{|\mathbf{n}\times\mathbf{k}|}k_z\Delta.\end{aligned} \tag{B-13}$$

The angle Δ has the same physical meaning as in 2D — it is an angle in the symmetry-axis planes between the vector $\mathbf{n}$ and $\mathbf{k}$. Therefore, as in 2D, the angle Δ is linearly dependent on ε' and δ'.

From the analogy to 2D (Equation B-6), one knows that the angle Δ is approximately proportional to

$$\sin\left(2\theta_{\mathbf{n},\mathbf{k}}\right) = 2\sin\left(\theta_{\mathbf{n},\mathbf{k}}\right)\cos\left(\theta_{\mathbf{n},\mathbf{k}}\right) = 2(\mathbf{n}\cdot\mathbf{k})|\mathbf{n}\times\mathbf{k}|, \tag{B-14}$$

with $\theta_{\mathbf{n},\mathbf{k}}$ being the angle between vectors $\mathbf{n}$ and $\mathbf{k}$. Here, the wave vector $\mathbf{k} = \{k_x, k_y, k_z\}$ and the symmetry axis vector $\mathbf{n} = \{n_x, n_y, n_z\} = \{\sin v\cos\alpha, \sin v\sin\alpha, \cos v\}$. One can then express the sum of the second and third terms in Equation B-12 as

$$\begin{aligned}\Delta U_{Px} &= -\frac{(\mathbf{n}\times\mathbf{k})_z}{|\mathbf{n}\times\mathbf{k}|}k_y\Delta + \frac{(\mathbf{n}\times\mathbf{k})_y}{|\mathbf{n}\times\mathbf{k}|}k_z\Delta \\ &= \frac{\Delta}{|\mathbf{n}\times\mathbf{k}|}\left[-(\mathbf{n}\times\mathbf{k})_z k_y + (\mathbf{n}\times\mathbf{k})_y k_z\right] \\ &= (a\varepsilon' + b\delta')(\mathbf{n}\cdot\mathbf{k})\left[-(\mathbf{n}\times\mathbf{k})_z k_y + (\mathbf{n}\times\mathbf{k})_y k_z\right] \\ &= (a\varepsilon' + b\delta')\left(n_x k_x + n_y k_y + n_z k_z\right) \\ &\quad\times\left[-\left(k_y n_x - k_x n_y\right)k_y + \left(k_x n_z - k_z n_x\right)k_z\right] \\ &= (a\varepsilon' + b\delta')\sum_{i\le j}\sum_{j=1}^{3} d_{ij}n_i n_j,\end{aligned} \tag{B-15}$$

where a, b, d_{ij} are functions of the vector $\mathbf{k}$. All components of $\Delta\mathbf{U}_P$ can be represented in this form. One can verify that this equation reduces to the 2D Equation B-7 by setting $k_y = 0$ and $\alpha = 0$. With this equation, one can interpolate the P mode in 3D similar to 2D.

The SV-mode can be interpolated in a way similar to the P-mode. Assuming that $\mathbf{U}^0_{\mathbf{SV}}(\mathbf{k})$ is the SV-mode polarization vector of an isotropic medium for a given wave vector $\mathbf{k}$, the TI polarization vector for SV-mode $\mathbf{U}_{\mathbf{SV}}$ is a rotation from $\mathbf{U}^0_{\mathbf{SV}}$, represented by a rotation matrix $\mathbf{R}_{\mathbf{SV}}$. Fortunately, because P- and SV-modes are mutually orthogonal and both are polarized in the same symmetry-axis plane for a given wave vector $\mathbf{k}$, the rotation matrix from $\mathbf{k}$ to $\mathbf{U}_{\mathbf{P}}$ and from $\mathbf{U}^0_{\mathbf{SV}}(\mathbf{k})$ to $\mathbf{U}_{\mathbf{SV}}$ are the same. By analogy, we have

$$\mathbf{U}_{SV} = \mathbf{R}(\mathbf{u})\mathbf{U}^0_{\mathbf{SV}}(\mathbf{k}), \tag{B-16}$$

and

$$\begin{aligned}U_{SVx} &= U^0_{SVx} - zk_y\Delta + yk_z\Delta \\ U_{SVy} &= U^0_{SVy} - xk_z\Delta + zk_x\Delta \\ U_{SVz} &= U^0_{SVz} - yk_x\Delta + xk_y\Delta.\end{aligned} \tag{B-17}$$

Therefore, the SV-mode can be obtained by interpolation in the same way as for the P-mode.

From Equation B-15, one can interpolate P and SV modes with

$$M = \left(1 - \sum_{k=1}^{N} w^k\right)M^0 + \sum_{k=1}^{N}\left(w^k M^k\right) = \sum_{k=0}^{N} w^k M^k, \tag{B-18}$$

where $M^0 = \mathcal{F}^{-1}\{\sum_{j=1}^{2} i\tilde{W}_j U^0_{Mj}\}$ is the separation with $\varepsilon = 0$ and $\delta = 0$ and $M^k = \mathcal{F}^{-1}\{\sum_{j=1}^{2} i\tilde{W}_j U^k_{Mj}\}$ is the separation with reference model at reference model $\mathbf{m}^k = \{\varepsilon^k, \delta^k, v^k, \alpha^k\}$.

REFERENCES

Aki, K., and P. Richards, 2002, Quantitative seismology (second edition): University Science Books.

Alkhalifah, T., 1998, Acoustic approximations for processing in transversely isotropic media: Geophysics, **63**, 623–631, doi:10.1190/1.1444361.

Bale, R. A., S. H. Gray, and M. Graziella, 2007, TTI wave-equation migration: 77th Annual International Meeting, SEG, Expanded Abstracts, **26**, 2295–2299.

Dellinger, J., 1991, Anisotropic seismic wave propagation: Ph.D. thesis, Stanford University.

Dellinger, J., and J. Etgen, 1990, Wave-field separation in two-dimensional anisotropic media: Geophysics, **55**, 914–919, doi:10.1190/1.1442906.

Etgen, J. T., and S. Brandsberg-Dahl, 2009, The pseudo-analytical method: Application of pseudo-laplacians to acoustic and acoustic anisotropic wave propagation: 79th Annual International Meeting, SEG, Expanded Abstracts, 2552–2556.

Fowler, P. J., X. Du, and R. P. Fletcher, 2010, Coupled equations for reverse time migration in transversely isotropic media: Geophysics, **75**, no. 1, S11–S22, doi:10.1190/1.3294572.

Gazdag, J., and P. Sguazzero, 1984, Migration of seismic data by phase shift plus interpolation: Geophysics, **49**, 124–131, doi:10.1190/1.1441643.

Liu, F., S. A. Morton, S. Jiang, L. Ni, and J. P. Leveille, 2009, Decoupled wave equations for p and sv waves in an acoustic VTI media: 79th Annual International Meeting, SEG, Expanded Abstracts, 2844–2848.

Shepard, D., 1968, A two-dimensional interpolation function for irregularly-spaced data: ACM '68: Proceedings of the 1968 23rd ACM National Conference, ACM, 517–524.

Stewart, R. R., J. Gaiser, R. J. Brown, and D. C. Lawton, 2003, Converted-wave seismic exploration: Applications: Geophysics, **68**, 40–57, doi:10.1190/1.1543193.

Tsvankin, I., 2005, Seismic signatures and analysis of reflection data in anisotropic media: 2nd edition: Elsevier.

Ursenbach, C., and R. Bale, 2009, TTI wave-equation migration for Canadian foothills depth imaging: The Leading Edge, **28**, 1344–1351, doi:10.1190/1.3259613.

Yan, J., and P. Sava, 2008, Isotropic angle-domain elastic reverse-time migration: Geophysics, **73**, no. 6, S229–S239, doi:10.1190/1.2981241.

——, 2009a, 3D elastic wave mode separation for TTI media: 79th Annual International Meeting, SEG, Expanded Abstracts, **28**, 4294–4298.

——, 2009b, Elastic wave-mode separation for VTI media: Geophysics, **74**, no. 5, WB19–WB32, doi:10.1190/1.3184014.

Zhang, Q., and G. A. McMechan, 2010, 2D and 3D elastic wavefield vector decomposition in the wavenumber domain for VTI media: Geophysics, **75**, no. 3, D13–D26, doi:10.1190/1.3431045.